

2-layer and 3-layer fiber geometry model based analysis of refractive index sensitivity of long period fiber grating with reduced cladding

S. PRASHAR^{a,b,*}, S. SINGH^a, D. ENGLER^b, S. KAUSHIK^c

^aChitkara University School of Engineering and Technology, Chitkara University, Himachal Pradesh, 174103, India

^bDepartment of Electronics Technology, Guru Nanak Dev University, Amritsar, Punjab, 143005, India

^cCentral Scientific Instruments Organization, Sector-30C, Chandigarh, 160030, India

This study investigates the refractive index (RI) sensitivity of long period fiber grating (LPFG) by means of 2-layer (2L) and 3-layer (3L) geometry models of optical fiber separately, through mathematical modelling. In order to realize the impact of particularly adopted model on measurement of RI sensitivity, the LPFG response is studied at reduced cladding radius. The reduction in cladding thickness increases the effect of ambient refractive index (ARI) on modal field distribution and improves sensitivity. However reducing cladding radius (up to 40.5 μm) decreases the cladding mode content of fiber. Such consequences affect the possible highest ordered cladding mode, so the highest order HE_{14} cladding has been chosen here for analysis. The RI sensitivity is evaluated in terms of coupled mode theory based transmission spectrum shift with respect to cladding radius. The obtained results of both fiber geometry models are compared with reported work to decide their authenticity.

(Received September 14, 2018; accepted June 14, 2019)

Keywords: Long period fiber grating, Fiber geometry model, Refractive index sensitivity

1. Introduction

Originally, LPFG is reported in 1994 [1]. Since then LPFG has marked its presence in variety of applications like: broad band optical coupler [2], mode dependent gain controller [3], twist sensor [4], humidity sensor [5], strain & temperature sensor [6] and refractive index (RI) sensor [7-9]. These applications are possible due to the control of LPFG over mode characteristics and propagating wavelength. As a result, LPFG response is assessed in terms of perturbation in the transmission spectrum of coupled cladding mode. The transmission profile of LPFG contains a series of attenuation bands due to the coupling of power in core mode to forward co-propagating cladding modes. The coupling between core and cladding modes is possible only when phase matching condition is satisfied at a resonant wavelength [10]. The phase matching condition depends on differential effective RI of coupled modes and the periodic modulation of few hundreds μm in the core region's RI [10-11]. Likewise, the differential effective RI is dependent on the geometrical characteristics of optical fiber and ambient medium refractive index (ARI) [7-11]. The geometrical model of optical fiber is obligatory to understand the structure and design parameters of LPFG. There are eigenvalue equations based on 2-layer (2L) [11] and 3-layer (3L) fiber geometry models [10,12] to estimate effective refractive indices (ERIs) of core and cladding modes. Such fiber geometry models have been analyzed by researchers [7-8,13-14] with reduced cladding, however they have calculated ERI of core mode

on the basis of 2L geometry model and ERI of cladding mode on the basis of 3L geometry model. Though, cladding thickness influences the interaction between ARI and core mode field, and is not ignorable [12]. The inclusion of cladding thickness effect on core mode ERI is possible by adopting 3L geometry model which inherits the contribution of ARI in it [15].

In this study, the modal characteristics of core and cladding modes have been analyzed individually based on 2L and 3L geometry models. The 3L geometry model has been used by the authors in literature to evaluate core mode ERI [16], however they have violated the condition of weakly guiding approximation in their analysis. This condition is obeyed in this paper during core mode ERI evaluation. Further, the LPFG RI sensitivity is evaluated using both geometry models separately, to ease up the selection of better geometry model for LPFG ARI sensor design. The position of resonance spectrum relies on cladding thickness dependent interactions of ARI with the modal field distribution of coupled core-cladding modes [7-8,13-14]. Consequently, the sensitivity is assessed in terms of positional shifting of resonant wavelength per unit ARI. The attributes of single mode fiber (SMF28e) are implemented in LPFG modeling by reducing cladding radius (a_{cl}) up to 40.5 μm for ARI from 1 to 1.454. The reduction of a_{cl} influences the number of cladding modes, for that reason HE_{14} cladding mode is considered which is the highest ordered cladding mode supported by SMF28e at $a_{cl} = 40.5\mu\text{m}$. The characteristics of coupled modes with reduced cladding are studied on the basis of vector coupled mode theory. The obtained results support

enhancement in ARI sensitivity by reducing a_{cl} and divulges 3L geometry model as a best choice for mathematical designing of LPFG.

2. Theoretical formulation

2.1. LPFG principle

LPFG is a part of few centimeters long core region of SMF having uniform periodic deformations from 100 to 1000 μm . Due to these periodic deformations, LPFG couples the light power in core mode to forward propagating cladding mode. The total electric field of the coupled light power is,

$$E(x) = [A_{co,01}(x) \exp\{-j(\delta_{01-1p} - \beta_{co})x\}] + [A_{cl,1p}(x) \exp\{j(\delta_{01-1p} + \beta_{cl,1p})x\}] \quad (1)$$

where, $A_{co,01}$ and $A_{cl,1p}$ are the amplitudes of core mode at incidence and co-propagating cladding mode along the grating length ($0 \leq x \leq G_L$), respectively. $\delta_{01-1p} = (1/2)\{\beta_{co} - \beta_{cl,1p}\} - (\pi/\Lambda_0)$ is detuning parameter which define the deviation of attenuation bands at resonant wavelength, here Λ_0 is the grating period. $\beta_{co} = (k_0 n_{co,eff})$ and $\beta_{cl,p} = (k_0 n_{cl,eff}^{1p})$ are the propagation constants of core and p^{th} cladding mode, respectively, where $k_0 = 2\pi/\lambda_j$ is free space propagation constant. The wavelength at which the fields of core and cladding modes couples and generate attenuation bands [10-11],

$$\lambda_c^{1p} = \Lambda_0 \{n_{co,eff}(\lambda_j) - n_{cl,eff}^{1p}(\lambda_j)\} \quad (2)$$

where, Λ_0 , $n_{co,eff}$ and $n_{cl,eff}^{1p}$ are grating period, core mode ERI and p^{th} cladding mode ERI at wavelength λ_j , respectively. The ERIs of core and cladding modes are functions of fiber's RIs for respective interfacing layers and geometrical characteristics.

2.2. Ambient medium RI sensitivity

In Eq. (2), the grating period does not vary with the change in ARI. Besides this, in 2L geometry model, only $n_{cl,eff}^{1p}$ is a function of ARI (n_{am}) and $n_{co,eff}$ remains constant with ARI [12], but in case of 3L geometry both $n_{co,eff}$ and $n_{cl,eff}^{1p}$ are functions of ARI. Therefore, for RI sensing the variation in ARI directs shift in coupling wavelength as,

$$\frac{d\lambda_c^p}{dn_{am}} = \frac{d\lambda_c^p}{d\delta n_{eff}^p} \left\{ \frac{dn_{co,eff}}{dn_{am}} - \frac{dn_{cl,eff}^{1p}}{dn_{am}} \right\} \quad (3)$$

where, $\delta n_{eff}^p = n_{co,eff} - n_{cl,eff}^{1p}$ (differential effective RI). In Eq. (3), on right hand side the derivative outside bracket emphasizes the shift in wavelength with respect to cladding mode order and the first & second derivatives

in the bracket indicates the variation of $n_{co,eff}$ and $n_{cl,eff}^{1p}$ with ARI, respectively.

2.3. ERI of core and cladding modes

2.3.1. Core mode ERI

Weakly Guiding approximation has been applied on the respective dispersion relations to evaluate ERIs of core mode and cladding modes. According to this approximation, the relative index difference of SMF must be low enough so that core mode ERI exists amidst the RI range $n_{cl} < n_{co,eff} < n_{co}$ and core mode remains guided in the core region. The 2L geometry is readily used in literature to evaluate core mode. The dispersion relation obtained through this geometry is limited to modal fields at core-clad interface in which ambient medium interaction with fields is neglected (see Fig. 1). The reason is large cladding region compared to core region, which ensures zero interaction of the field in core mode with ambient medium. So, the dispersion relation for core mode conferring to 2L geometry model is [10],

$$V_{12}\sqrt{1-b}[J_1(V_{12}\sqrt{1-b})/J_0(V_{12}\sqrt{1-b})] = V_{12}\sqrt{b}[K_1(V_{12}\sqrt{b})/K_0(V_{12}\sqrt{b})] \quad (4)$$

Here, $J_{()}$ and $K_{()}$ the Bessel functions of first kind and modified Bessel function of second kind, respectively. V_{12} (normalized transverse phase constant) $= (2\pi a_{co}/\lambda)\sqrt{n_{co}^2 - n_{cl}^2}$ and $b = (n_{co,eff}^2 - n_{cl}^2)/(n_{co}^2 - n_{cl}^2)$, where a_{co} is core radius, n_{co} and n_{cl} represent refractive indices of core and cladding regions, respectively.

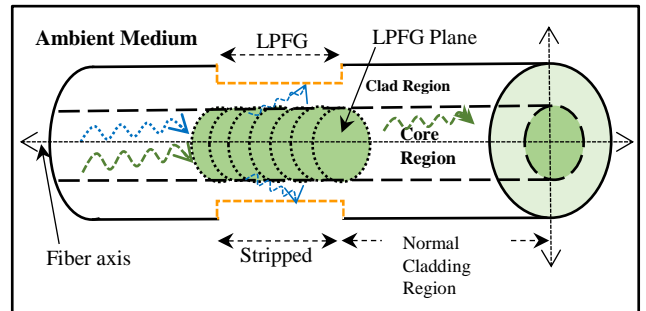


Fig. 1. Design of modelled LPFG

On the other hand, in an intention to consider the interactions between ARI and core mode field, the fields at clad-ambient medium interface must be considered. Also, the reduction in cladding thickness excites the interaction between ARI and core mode field. Therefore, in these situations, a 3-layer geometry model based optical fiber structure is useful for core mode evaluation. The 3-layer geometry based eigenvalue equation for core mode is [12],

$$\begin{aligned}
 & P_v^2 - \{(a_{co}/a_{cl}W_{co}^2)\}^2(n_{cl}^2/n_{co}n_{am})Y_1Y_2 + \\
 & Y_1^2Y_2^2\{J_a(K_aP_v - R_v a_{co}/a_{cl}W_{co}) + (1/W_{co})(K_aQ_v - \\
 & S_v a_{co}/a_{cl}W_{co})\}\{J_a(K_aP_v - R_v s_{23}a_{co}/a_{cl}W_{co}) + \\
 & (s_{21}/W_{co})(K_aQ_v - S_v s_{23}a_{co}/a_{cl}W_{co})\} - Y_1^2(J_aP_v - \\
 & Q_v/W_{co})(J_aP_v - s_{21}Q_v/W_{co}) - Y_2^2(K_aP_v - \\
 & R_v a_{co}/a_{cl}W_{co})(K_aP_v - R_v s_{23}a_{co}/a_{cl}W_{co}) = 0
 \end{aligned} \quad (5)$$

Here,

$$\begin{aligned}
 P_v &= I_v(W_{cl})K_v(W_{co}) - I_v(W_{co})K_v(W_{cl}), \\
 Q_v &= I_v(W_{cl})K'_v(W_{co}) - I'_v(W_{co})K_v(W_{cl}), \\
 R_v &= I'_v(W_{cl})K_v(W_{co}) - I_v(W_{co})K'_v(W_{cl}), \\
 S_v &= I'_v(W_{cl})K'_v(W_{co}) - I'_v(W_{co})K'_v(W_{cl}), \\
 J_a &= \{J'_v(U_{co})/U_{co} J_v(U_{co})\}, \\
 K_a &= \{K'_v(W_{cl})/W_{cl} K_v(W_{cl})\},
 \end{aligned}$$

$$\begin{aligned}
 U_{co} &= a_{co}k_0\sqrt{n_{co}^2 - n_{co,eff}^2}, W_{co} = a_{co}k_0\sqrt{n_{co,eff}^2 - n_{cl}^2}, \\
 W_{cl} &= a_{cl}k_0\sqrt{n_{co,eff}^2 - n_{am}^2}, s_{21} = n_{cl}^2/n_{co}^2, s_{23} = \\
 & n_{cl}^2/n_{am}^2, V_{23} = a_{cl}k_0\sqrt{n_{cl}^2 - n_{am}^2}, Y_1 = \\
 & u_{co}a_{co}^2W_{co}^2/\gamma_0V_{12}^2, Y_2 = n_{cl}a_{cl}^2W_{co}^2W_{cl}^2/\gamma_0a_{co}^2V_{23}^2 \text{ and} \\
 & \gamma_0 = v\beta_{co}/k_0.
 \end{aligned}$$

where, J_v , K_v and I_v are the Bessel functions of first kind, modified Bessel function of second kind and modified Bessel function of first kind, respectively; a_{cl} is cladding radius.

2.3.2. Cladding mode ERI

In both types of fiber geometry models, the cladding modes' ERIs occur within the RI range $n_{am} < n_{cl,eff}^{1p} < n_{cl}$, means $n_{cl,eff}^{1p}$ is reliant on the variations of ARI [10-11]. With the aim of $n_{cl,eff}^{1p}$ estimation by 2L geometry model, the modal fields only at the clad-ambient medium interface are considered. The core region which has minimum area of concern as compared to other two regions (clad region and ambient medium region) is neglected under this analysis. Due to all these assumptions of 2L geometry, now Fig. 1 can be visualized as a multimode step index optical fiber structure. However, in a sense to include interactions of fields at core-clad interface in $n_{cl,eff}^{1p}$ calculation, a 3L geometry model based fiber structure is a right choice (Fig. 1) [15]. The three layers of this model are core region, clad region and ambient medium region.

Here, for $n_{cl,eff}^{1p}$ estimation using both types of fiber structures, the well-known dispersion relations given in the literature of references 11 (for 2L model) and 10 (for 3L model) have been implemented.

3. Results and validation

Two types of optical fiber geometry models are investigated on the schematic diagram of cladding reduced LPFG shown in Fig. 1. To calculate core mode and cladding mode ERIs at different cladding radius, the used specifications of SMF28e are $a_{co} = 4.1\mu\text{m}$, $a_{cl} = 62.5\mu\text{m}$, $n_{co} = 1.46145$, $n_{cl} = 1.456$ and free space wavelength = 1360nm [6,17]. In this analysis, firstly, the ERIs of core and cladding modes are evaluated and then the RI sensitivity is assessed independently using both the geometry models.

3.1. Analysis of $n_{co,eff}$ and $n_{cl,eff}^{1p}$

In Fig. 2, the evaluated $n_{co,eff}$ w.r.t. cladding radius (a_{cl}) on the basis of 2L and 3L geometry models are almost same for $a_{cl} \geq 45\mu\text{m}$. However, for $a_{cl} < 45\mu\text{m}$, the 3L based evaluation has shown gradual decrease in value of core mode ERI and strangely sudden decrease in it for a_{cl} below $20\mu\text{m}$. Contrary to which, 2L geometry model provides constant core mode ERIs for whole range of cladding radius ($62.5\mu\text{m}$ to $8.5\mu\text{m}$). In other words, 2L geometry model does not include the impact of cladding reduction and perturbation in ARI while calculating ERI. Whereas, in case of 3L model, the continuous decrease of ERI has proved that there is increase in the effect of specific ARI on core mode field distribution with reduction in cladding thickness. Meanwhile, for $a_{cl} < 20\mu\text{m}$, the sudden decrease in ERI narrates that ARI influences core mode field distribution more at lower values of cladding radius. One more notable information about ARI interference is that when ARI nears to cladding RI, core mode ERI increases with cladding radius decrement. Under such conditions, it is also observed that ERIs of all cladding modes follow same trend of value increment. Hence, 3L geometry model is more suitable to include the role of cladding thickness as well as ARI in core mode assessment.

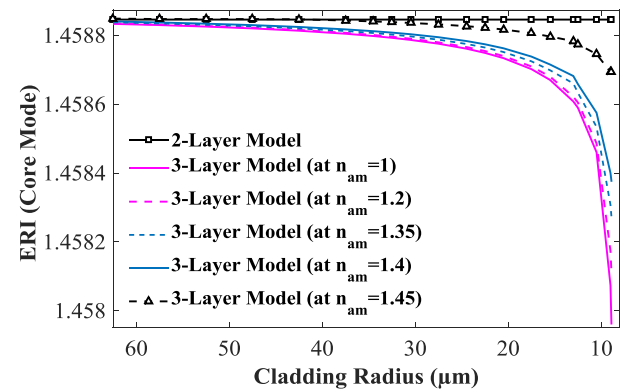


Fig. 2. Comparison of $n_{co,eff}$ on cladding radius at different ARIs

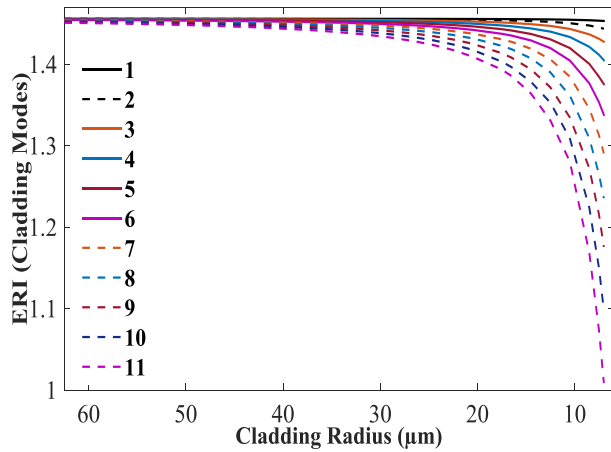


Fig. 3. Effect of cladding thickness on cladding mode ERI at ARI=1 (2L geometry)

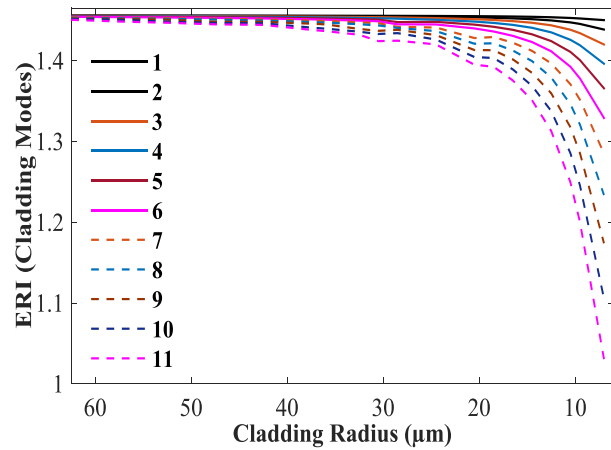


Fig. 4. Effect of cladding thickness on cladding mode ERI at ARI=1 (3L geometry)

It has been assumed in cladding mode estimation that azimuthal number (v) is 1, so that in LPFG the circular

symmetric RI modulation remains transverse with respect to optical fiber axis, an essential condition for non-zero coupling coefficients between core and cladding modes [10]. Addition to this, the coupling strength between the core mode and odd ordered cladding mode is higher than the coupling strength between core mode and even ordered cladding mode [10]. Hence, only odd ordered modes have been considered in this study. The comparison of $n_{cl,eff}^{1p}$ values calculated using 2L and 3L geometry models differ from each other at fourth decimal place which extends to second decimal place when $a_{cl} \sim 10 \mu m$. Fig. 3 and 4 describe the decrease in $n_{cl,eff}^{1p}$ of odd ordered HE_{vp} cladding modes ($p=1-11$) at slower rate for $a_{cl} \geq 40 \mu m$ and at faster rate for $a_{cl} < 28 \mu m$ at $ARI=1$. The behavior of $n_{cl,eff}^{1p}$ reports the increase in the influence of ARI on cladding mode's field distribution and maximum at lower end of cladding radius i.e. for $a_{cl} < 28 \mu m$. Moreover, with the increase in mode order the rate of decrease of $n_{cl,eff}^{1p}$ rises with cladding reduction. Means, the influence of ARI has been increased with cladding mode order and enforces to choose higher ordered modes for higher sensitivity attainment.

Furthermore, with the stripping of cladding, the amount of cladding modes in an SMF decreases. Table 1 shows the diminution in amount of fiber modes in cladding region with the reduction in its radius. The V_{23} parameter is responsible for this decrease, as V_{23} defines the number of modes supported by cladding region and is directly proportional to a_{cl} [11]. The reduction in a_{cl} decreases V_{23} as well as amount of cladding modes in optical fiber and subsequently, sets a limit at the probable highest order cladding mode. It has been also observed that lowest number of cladding modes are present at ARI near to n_{cl} as that of at ARI with low value (table I). This is due to the dependency of V_{23} parameter on differential RI of interfacing layers.

Table 1. Total number of cladding modes supported by an optical fiber at different ARI

| Cladding Radius (μm) | Number of cladding modes at ARI (1-1.454) | | | | | | | | | | |
|-----------------------------|---|-----|-----|------|------|------|------|-------|-------|-------|-------|
| | 1 | 1.2 | 1.3 | 1.35 | 1.41 | 1.42 | 1.43 | 1.442 | 1.448 | 1.452 | 1.454 |
| 52.5 | 68 | 56 | 51 | 42 | 24 | 21 | 18 | 14 | 11 | 8 | 5 |
| 42.5 | 50 | 41 | 37 | 32 | 20 | 19 | 15 | 11 | 9 | 6 | 4 |
| 32.5 | 46 | 37 | 28 | 23 | 16 | 15 | 12 | 9 | 7 | 5 | 3 |
| 16.5 | 24 | 19 | 15 | 12 | 8 | 7 | 6 | 4 | 3 | 2 | 1 |
| 8.5 | 12 | 9 | 7 | 6 | 4 | 3 | 3 | 2 | 1 | 1 | 0 |

Table 2. Comparison of ARI sensitivities of HE_{14} cladding mode for ARI (1-1.454)

| ARI Range | Sensitivity nm/RIU (2-Layer Model) at a_{cl} | | | Sensitivity nm/RIU (3-Layer Model) at a_{cl} | | |
|-------------|--|--------------|--------------|--|--------------|--------------|
| | 62.5 μm | 50.5 μm | 40.5 μm | 62.5 μm | 50.5 μm | 40.5 μm |
| 1-1.2 | 1.0 | 1.7 | 7.2 | 1.8 | 3.8 | 16.2 |
| 1.2-1.3 | 2.9 | 9.6 | 16.5 | 3.5 | 13.5 | 32.4 |
| 1.3-1.395 | 14.4 | 22.1 | 46.8 | 16.4 | 27.1 | 72.8 |
| 1.395-1.438 | 54.1 | 115.6 | 230.1 | 61.5 | 165.4 | 381.4 |
| 1.438-1.452 | 473.5 | 935.7 | 1915.8 | 576.0 | 1393.3 | 3330.7 |
| 1.452-1.454 | 2900.4 | 6203.2 | 16637.5 | 4430.3 | 10328.7 | 24207.2 |
| 1-1.454 | 37.6 | 75.6 | 170.8 | 47.0 | 113.5 | 275.0 |

3.2. RI sensitivity analysis based on both models

The specifications of designed LPFG are $\Lambda_0=550\mu\text{m}$, $G_L=25\text{mm}$ and Δn (modulation index) = 2.5×10^{-4} . Fig. 5 & 6 validate the displacement of resonant wavelengths towards longer wavelength (red shift) with the reduction in cladding radius. It is observed from Fig. 6 that the existence of resonant wavelengths of HE_{14} cladding mode

is at more longer wavelengths with the reduction in cladding for 3L geometry model. The cause of red shift is decrease in ERIs of core and cladding modes with the reduction in cladding radius. However, the rate of decrease in core mode ERIs is very low and zero as compared to cladding mode ERIs for 3L and 2L geometry models, respectively.

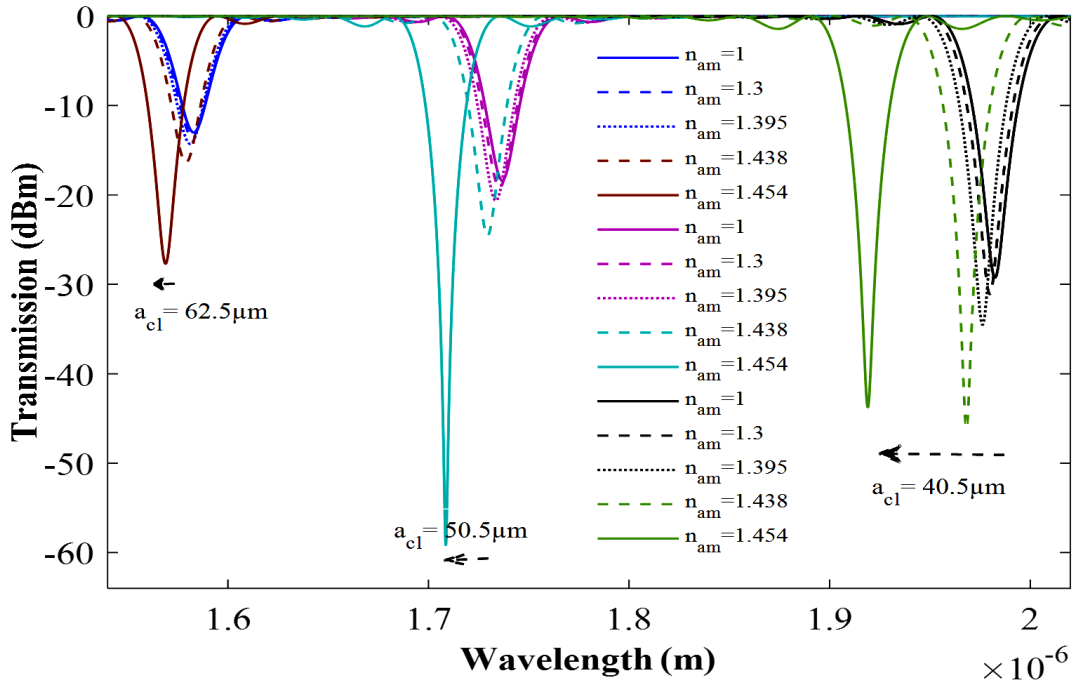


Fig. 5. LPFG's transmission spectra for HE_{14} cladding mode at different cladding radii (2-Layer Geometry).

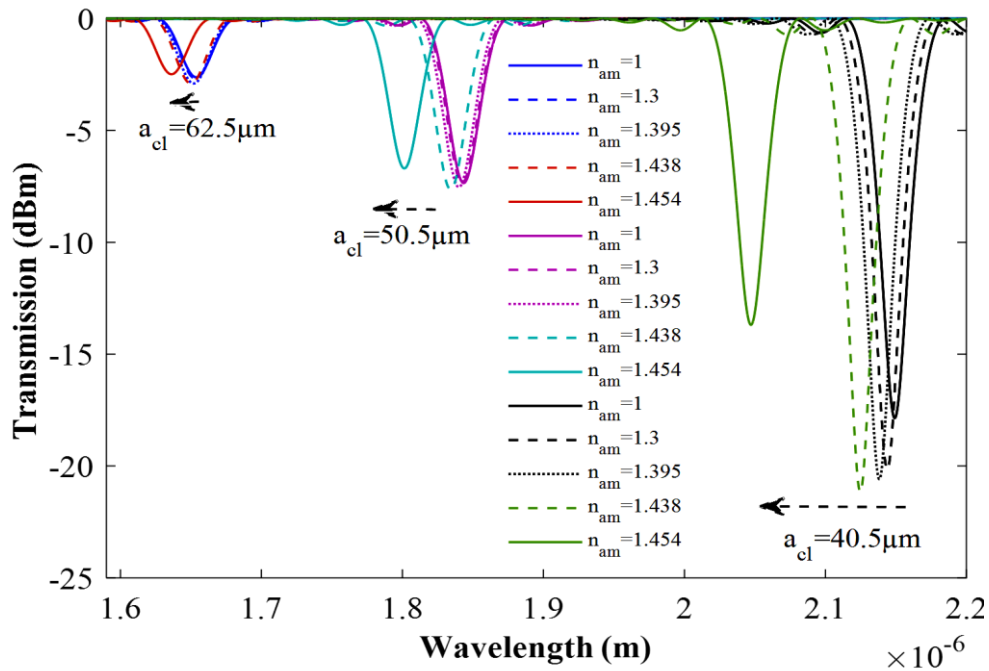


Fig. 6. LPFG's transmission spectra for HE_{14} cladding mode at different cladding radii (3-Layer Geometry)

Additionally, the blue shift of attenuation bands for ARI range 1-1.454 in Figs. 5 and 6 is due to rise in cladding mode ERIs with ARI. It is also seen that the coupling strength has increased with decrease in cladding radius. All attenuation depths in spectral profile have variations due to modulation in coupling strengths with ARI at different cladding radii. In 3L approach, a decline in the magnitude of attenuation band depth has been observed for ARI near to cladding RI. This is due to the general process of cladding mode power recoupling to core region of fiber gratings [10]. The same behavior is not shown by the spectra of 2L geometry model. Thus, the variations in attenuation depths is more logical and symmetric in case of 3L geometry model in comparison to 2L geometry model.

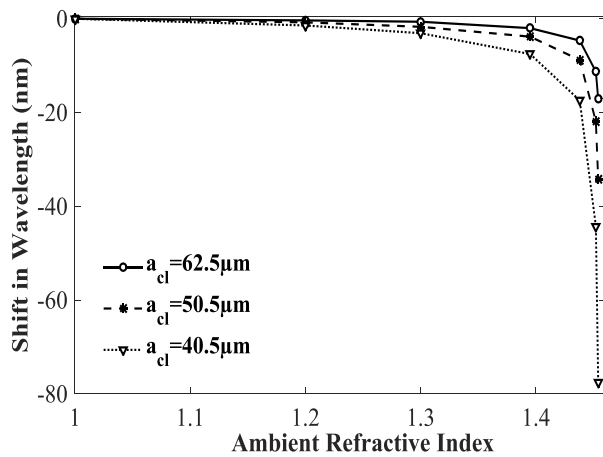


Fig. 7. LPFG's RI response with ARI (1-1.454) at different cladding radii (2-Layer Geometry).

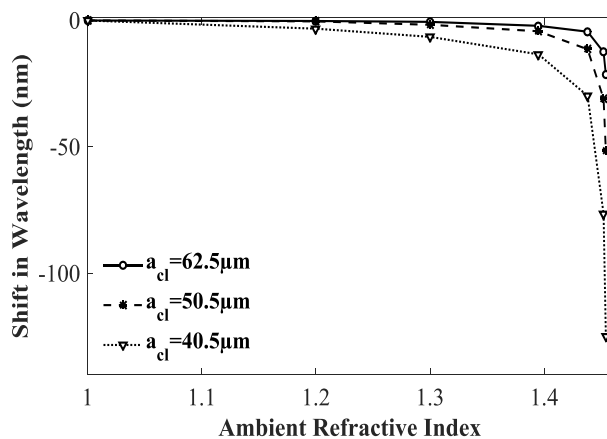


Fig. 8. LPFG's RI response with ARI (1-1.454) at different cladding radii (3-Layer Geometry).

In Figs. 7 & 8 the shift in wavelength is increasing with the reduction in a_{cl} . Moreover, 3L geometry model implores larger shift in wavelength as compared to 2L geometry model with ARI and a_{cl} . The attainment of larger shift in coupling wavelength emphasizes on the

improvement in sensitivity and RI resolution. Such responses signify the increased impact of ARI on modal field distribution with cladding reduction. In case of normal LPFG, the maximum shift has been found for ARI which is in close vicinity of cladding RI, but at small cladding radii the ARI from 1.3-1.454 has captured maximum part of total wavelength shift.

These results project LPFG as a capable sensor to sense large number of chemicals. The difference in sensitivities in table II validate the increased scale of RI sensitivities obtained through 3L as compared to 2L geometry model and tabularizes highest at $a_{cl} = 40.5\mu\text{m}$. The shift in wavelength using 3L geometry model is found to be quite similar to experimental results for HE_{14} mode in literature (Ref. 17) at $a_{cl} = 62.5\mu\text{m}$.

4. Conclusion

Our investigation shows noteworthy difference between the RI responses associated to 2L and 3L geometry models. It is apparent from the analysis of 3L geometry model that ERI of core mode changes with decrease in cladding radius while for similar analysis with 2L geometry model, remains constant. Therefore, on the basis of 3L geometry model core mode ERI becomes a function of ARI. Moreover, the core mode ERIs have religiously followed weakly guided approximation in this study which was not considered in earlier literature [16]. It is also found that the probable highest ordered cladding mode is dependent on the difference between ARI and cladding RI along with cladding radius. In addition, the RI sensitivities with 2L geometry model are found lower than 3L geometry model. The 3L geometry model reports highest RI sensitivity at $a_{cl} = 40.5\mu\text{m}$ which is approximately 5.8 times higher than a_{cl} at $62.5\mu\text{m}$. Therefore, designers are able to control RI sensitivity and index resolution by varying cladding thickness of LPFG RI sensor. Moreover, 3L geometry model based response of HE_{14} cladding mode at $a_{cl} = 62.5\mu\text{m}$ is in agreement with the experimentally reported work in literature [17]. Finally, owing to the above findings, we support the 3L fiber geometry model as most appropriate approach for mathematical modeling of LPFG in case of ARI less than cladding RI.

Acknowledgements

Authors are thankful to Ms. Rohini Rai and Mr. Vinamar Prashar for their suggestions in formatting of this paper.

References

- [1] C. D. Poole, H. M. Presby, J. P. Meester, Electron.

- Lett. **30**, 1437 (1994).
- [2] Y. Liu, K. S. Chiang, IEEE Photonics Technology Letters **18**, 229 (2006).
- [3] M. Wada, T. Sakamoto, T. Mori, T. Yamamoto, N. Hanzawa, F. Yamamoto, J. Lightwave Technol. **32**, 4092 (2014).
- [4] R. Gao, Y. Jiang, L. Jiang, Opt. Express **22**, 15679 (2014).
- [5] H. Liu, H. Liang, M. Sun, K. Ni & Y. Jin, IEEE Sens. J. **14**, 893 (2014).
- [6] S. Prashar, D. Engles, S.S. Malik, Photonic. Netw. Commun. **35**, 258 (2018).
- [7] K. Chiang, Y. Liu, M. Ng, X. Dong, Electron. Lett. **36**, 966 (2000).
- [8] A. Iadicicco, S. Campopiano, M. Giordano, A. Cusano, Appl. Optics **46**, 6945 (2007).
- [9] R. Garg, S. M. Tripathi, K. Thyagarajan, W. J. Bock, Sensor. Actuat. B **176**, 1121 (2013).
- [10] T. Erdogan, J. Opt. Soc. Am. A **14**, 1760 (1997).
- [11] A. M. Vengsarkar, P. J. Lemaire, J. B. Judkins, V. Bhatia, T. Erdogan, J. E. Sipe, J. Lightwave Technol. **14**, 58 (1996).
- [12] Z. Zhang, W. Shi, J. Opt. Soc. Am. A **22**, 2516 (2005).
- [13] K. Zhou, H. Liu, X. Hu, Opt. Commun. **197**, 295 001).
- [14] K. Chung, S. Yin, Opt. Lett. **29**, 812 (2004).
- [15] S. Prashar, D. Engles, S. S. Malik, Microwave. Opt. Technol. Lett. **59**, 658 (2017)
- [16] H. Chen, Z. Gu, J. Mod. Optic. **58**, 1659 (2011).
- [17] T. M. Libish, M. C. Bobby, J. Linesh, P. Biswas, S. Bandyopadhyay, K. Dasgupta, P. Radhakrishnan, J. Optoelectron. Adv. M. **13**(5), 491 (2011).

*Corresponding author: shivendu.prashar@gmail.com